Atomic structure of the icosahedral Al-Li-Cu quasicrystal

1991 J. Phys.: Condens. Matter 3 1

(http://iopscience.iop.org/0953-8984/3/1/001)

J. Phys.: Condens. Matter 3 (1991) 1–25. Printed in the UK

Atomic structure of the icosahedral Al–Li–Cu quasicrystal

M de Boissieu†‡, C Janot†, J M Dubois§, M Audier‡ and B Dubost‖
‡ Institut Laue–Langevin, 156X, 38042 Grenoble Cédex, France
‡ LTPCM-ENSEEG, BP 75, 38402 St Martin d'Hères Cédex, France
§ LSG2M, Ecole des Mines, Parc de Saurupt, 54042 Nancy Cédex, France
‖ Pechiney, Centre de Recherches, BP 27, 38340 Voreppe, France

Received 23 February 1990, in final form 2 October 1990

Abstract. Using both powder and single crystal samples, neutron and x-ray diffraction data were obtained with quasicrystals of the AlLiCu system. Isotopic substitution on the Li and Cu atomic sites allowed amplitudes and phase shift of the partial structure factors to be determined. Using a high-dimensional crystallography approach results in the phases to be reconstructed and atomic densities were calculated. The six-dimensional periodic structure appeared as a primitive hypercubic lattice with mid-edge and vertex Al/Cu atomic surfaces plus a Li bodycentre site. The major drawbacks of the experimental approach are then bypassed by modelling details of the six-dimensional structure, still in agreement with diffraction data. The related three-dimensional quasiperiodic structure can be described in terms of connected clusters or, alternatively, families of atomic planes. Comparison with the structure of the crystalline R-phase is of interest.

1. Introduction

In periodic crystals the structure is completely specified when both the unit cell (or the Bravais lattice) and the positions of atoms in this unit cell are determined. The so-called direct methods of crystallography are the usual way to extract this structural information from diffraction data. Basically the structure is at first modelled rather crudely and then progressively refined by adjusting atomic coordinates to fit the diffraction data.

Quasiperiodic crystals actually have hidden translational invariances which can be recovered if the structure is properly specified in a higher dimensional space. For instance, icosahedral quasicrystals cannot have three-dimensional (3D) periodicity but there are 6D cubic Bravais lattices accepting these symmetries. Recovering periodic schemes at the expense of higher dimensionality allows the tools of crystallography to be used, although necessarily within a very careful approach, as made previously [1–4] with quasicrystals of the AlMn system [5]. This is, however, intrinsically more difficult for a quasicrystal than for a crystal. A perfect quasiperiodic structure, without any disorder, still has an infinite number of sites in 3D which are not exactly equivalent. There are also practical difficulties to be overcome, related to the fairly low level of information that can be extracted from diffraction patterns of quasicrystals.

One way to overcome these experimental difficulties partly, is to collect the largest possible number of independent sets of diffraction data with the aim of separating

0953-8984/91/010001 + 25 $03.50

chemical from topological parameters. Such a procedure has been achieved to some extent with the AlMn quasicrystals [1, 2] thanks to contrast variation effects in neutron diffraction.

Quasicrystals of the AlLiCu system are certainly an exciting subject within this scheme since contrast variations can be easily and rigorously produced by isotopic substitutions on Li(^{6}Li, ^{7}Li) and Cu(^{63}Cu, ^{65}Cu) atoms [6]. Moreover, single grains of more than a millimetre across [7–10] can be grown and then single crystal x-ray and neutron diffraction studies are feasible [11–14]. The purpose of this paper is to derive the best possible structure of AlLiCu quasicrystals, directly from neutron and x-ray diffraction data.

2. Basic principles for quasicrystallography

The relations between 3D quasiperiodic and higher dimensional periodic structures are well understood [15–17]. Icosahedral quasicrystals have periodic structures in 6D space which contains our 3D physical space, also called parallel space $R3_{par}$ and a complementary, or perpendicular, space $R3_{perp}$. In the cut method [18], an icosahedral quasiperiodic arrangement of atoms in 3D physical space $R3_{par}$ corresponds to a periodic arrangement of 3D hypersurfaces, or atomic shells $A3_{perp}$ in 6D space R6. These atomic shells intersect the 3D real world hyperplane at the atom positions. For each type (or family) of atomic sites in three dimensions there is one $A3_{perp}$ shell whose relative volume is directly related to the corresponding relative atomic 3D density. In an idealistic monoatomic icosahedral quasicrystal, with a single site at the origin of the 6D structure, and triacontahedral $A3_{perp}$ entirely contained in the $R3_{perp}$ space, the 3D atomic density is a distribution of Dirac functions at the vertex positions of a 3D Penrose tiling (3DPT). The volume of $A3_{perp}$ is equal to n_3a^6 in which a is the 6D lattice parameter and n_3 the 3D atomic density.

Correspondence rules also exist between the reciprocal spaces R6*, $R3^*_{par}$ and $R3^*_{perp}$. These reciprocal spaces contain the Fourier transforms (FT) of the densities. It is easy to demonstrate that the FT of the 3D density, i.e. $F(\boldsymbol{Q}_{par})$, is the projection onto $R3^*_{par}$ of the FT of the 6D density, i.e. $F(\boldsymbol{Q}_6)$, in R^*_6; $F(\boldsymbol{Q}_6)$ in turn is a distribution of δ-functions modulated by $G(\boldsymbol{Q}_{perp})$, the FT of $A3_{perp}$ ($\boldsymbol{Q}_{par}$ and $\boldsymbol{Q}_{perp}$ are the projections of $\boldsymbol{Q}_6$ onto $R3^*_{par}$ and $R3^*_{perp}$, respectively).

The points of interest for an experimental approach to the quasicrystal structures may then be summarized as follows.

(i) There is a one-to-one correspondence between $\boldsymbol{Q}_6$ and $\boldsymbol{Q}_{par}$ which generates a six integer indexing of the diffraction peaks measured at $\boldsymbol{Q}_{par}$ in $R3^*_{par}$ and allows us to derive from diffraction data the 6D Bravais lattice and possibly the space group in the case of favourable extinction rules [19, 20].

(ii) Intensities $|F(\boldsymbol{Q}_{par})|^2$ measured at $\boldsymbol{Q}_{par}$ in diffraction data are also the intensities $|F(\boldsymbol{Q}_6)|^2$ that would correspond to a '6D diffraction experiment'.

(iii) The diffraction pattern in $R3^*_{par}$ is a very dense set of peaks whose intensity is a decreasing function of $\boldsymbol{Q}_{perp}$.

(iv) The direct FT of these measured $F(\boldsymbol{Q}_6)$, or, at least of $|F(\boldsymbol{Q}_6)|^2$, gives the 6D structure (site positions *and* $A3_{perp}$ function), or at least the corresponding 6D Patterson functions [3, 4].

(v) The 3D cut of this 6D structure by $R3_{par}$ results in physical atom positions.

With ternary compounds such as AlLiCu quasicrystals, the $F(Q_{par})$ and $F(Q_6)$ structure factors contain several contributions such as

$$F(Q_6) = \delta(Q - Q_6^{lat}) \sum_{\alpha} b_\alpha G_\alpha(Q_{perp}) \exp(i2\pi Q_6 \cdot r_\alpha)$$

α being indicative of the atomic sites at position r_α in 6D space; b_α are the scattering lengths of atoms sited at r_α and G_α the FT of the pertinent volume $A3_{perp}(\alpha)$ attached to each site. The FT of these $F(Q_6)$ gives the lattice points in 6D correctly but it is generally difficult to extract $A3_{perp}(\alpha)$ atomic shells. Isotopic substitutions, when feasible, allow variation of the weight of one, or several, atomic species into the neutron diffracted intensities. By measuring several diffraction patterns weighted differently, it is then possible to calculate what would be the diffraction pattern if each atomic species was alone, i.e. the so-called *partial* structure factor. The problem can then be treated as the superposition of several monoatomic structures. This method is going to be used hereafter.

3. Sample preparation, alloy properties and experiments

Within the field of research for light AlLi–base alloys to be used for aerospace purposes, the AlLiCu phase diagram has been reconsidered carefully along with the thermodynamical properties of the phases of interest [21]. The identified phases were the tetragonal θ-Al_2Cu, FCC δ-AlLi, FCC TB-$Al_{7.5}Cu_4Li$, BCC R-Al_5CuLi_3, HEX Tl-Al_2CuLi and icosahedral T2-Al_6CuLi_3. In particular, it has been shown that only slow cooling rates are required to form the icosahedral T2-phase which behaves like an equilibrium phase going, apparently, directly to the liquid state upon heating. The T2-phase can be obtained as the grain boundary precipitates upon annealing in an aluminium-rich AlCuLi alloy, or by direct solidification of large dendrites embedded into an Al-rich matrix, or else, by free solidification into the single grain quasicrystal [8]. The phase diagram as reported in [21] shows that the BCC R-phase and the icosahedral T2-phase have very similar features. Their densities are almost the same (2.46 and 2.47 g cm^{-3}, respectively) and they form within a very narrow composition range: $Al_{5.60}Cu_{1.20}Li_{3.20}$ for the R-phase and $Al_{5.70}Cu_{1.08}Li_{3.22}$ for the T2-phase (within 3% error bars). The R-phase is likely to melt congruently at 638 ± 2 °C while the T2-phase undergoes a non-congruent melting at 622 ± 2 °C. A very unfortunate consequence is that a completely pure T2-phase cannot be obtained easily and one has to accept contamination by residual α-Al or (and) T1-phase except perhaps for the small triacontahedral single grains which result from free solidification with separation of the dendrites from the residual liquid in internal shrinkage cavities. This has to be kept in mind of course when analysing diffraction data from bulk samples, even if the point is somewhat dedramatized by the relatively small distance in the phase diagram between the true liquid–solid transition and the virtual congruent melting temperature of the T2 compound. Powder neutron diffraction patterns of both the T1 and ico-phases are shown in figure 1: they are going to be considered for a proper identification of the actual diffraction peaks of the icosahedral phase.

As already stated, neutron diffraction is particularly well suited when isotopic contrast variation can be achieved. Lithium has two stable isotopes, ^{6}Li and ^{7}Li, whose respective scattering lengths are $+0.20 \times 10^{-12}$ and -0.222×10^{-12} cm. This allows significant changes into the contrast on the Li sites of the structure when alloys are prepared with different ^{6}Li/^{7}Li mixtures. A 'zero-scatterer' element Li$^{(0)}$ is even easily

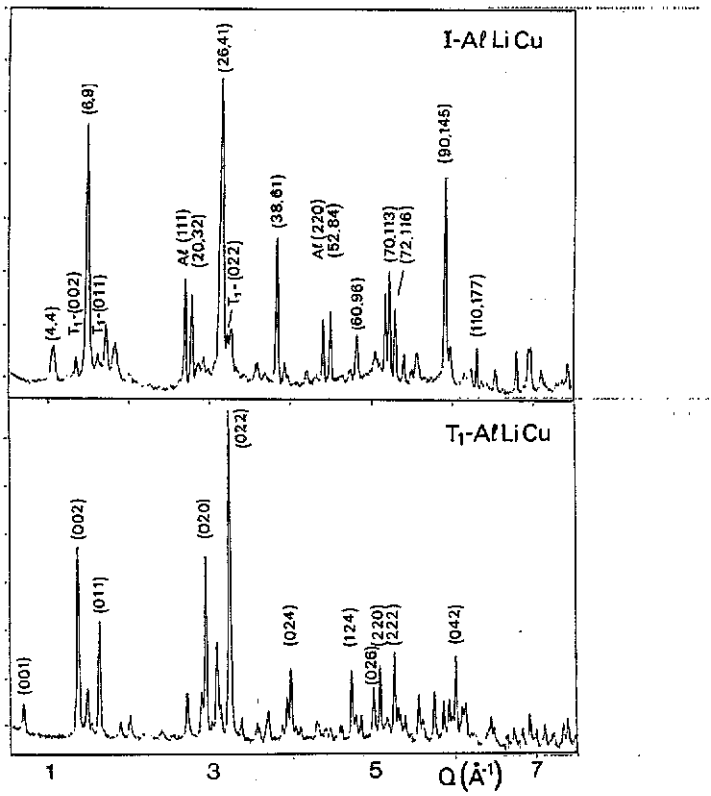

Figure 1. Neutron powder diffraction patterns as measured with the ico-phase (top) and the parasitic crystalline T_1-phase (bottom). The strongest peaks of T_1, (022), is visible in the ico-phase pattern and allows an estimate of the contamination. The ico-phase peaks are indexed with (N, M) according to [19].

obtained by mixing the two isotopes in a ratio of about 1 : 1. Copper also has two stable isotopes: ^{63}Cu with a scattering length of $+0.672 \times 10^{-12}$ cm and ^{65}Cu with a scattering length of $+1.102 \times 10^{-12}$ cm.

The ^{6}Li/^{7}Li mixtures, at different composition were chill cast from 250 °C into boron-nitride coated steel crucibles under an argon controlled atmosphere. The lithium mixture was then added to proper Al–Cu liquid alloys at 730 °C. The resulting AlCuLi liquid was finally chill cast within five minutes into preheated graphite-coated steel moulds and maintained at 500 °C for about 80 h in dry air. The solidified ingots of T2-phase (Φ= 18 × 60 mm) were ground into a fine powder and put into thin-walled vanadium containers for the purpose of powder neutron diffraction measurements. Five samples of the icosahedral phase were produced with natural copper and different ^{6}Li/^{7}Li isotopic compositions corresponding to ⟨Li⟩ scattering length b (Li) = −0.190 (natural Li), −0.110, 0, +0.102, +0.20 (pure ^{6}Li isotope) (in 10^{-12} cm), and two more samples with Li-zero scatterer (b(Li) = 0) and either ^{63}Cu or ^{65}Cu isotope.

Parts of the sample were characterized by powder x-ray diffraction and electron diffraction. The shrinkage cavity method already mentioned in this paper and described in detail elsewhere [8] was used to produce single (quasi)crystal grains and large pieces

of oriented dendrite of the icosahedral phase, for the purpose of four-circle x-rays and neutron diffraction scans.

The powder neutron diffraction data were collected at the high flux reactor facilities of the Institut Laue-Langevin (ILL, Grenoble), using the D2B two-axis diffractomer. We used it with a wavelength of the monochromatized neutron beam of $\lambda = 1.5947$ Å and in a high flux configuration that corresponds to a resolution $\Delta Q/Q \approx 5 \times 10^{-3}$. Diffraction patterns were accumulated over periods of 12 h. Data were treated as explained in detail elsewhere [1]. Diffraction patterns are shown in figure 2.

The single crystal x-ray diffracted intensities were collected on an AED2 Siemens four-circle diffractometer with a MoK_α ($\lambda = 0.7107$ Å) anode. The icosahedral single grain was a small triacontahedron of about 200 μm diameter. About 1000 diffracted

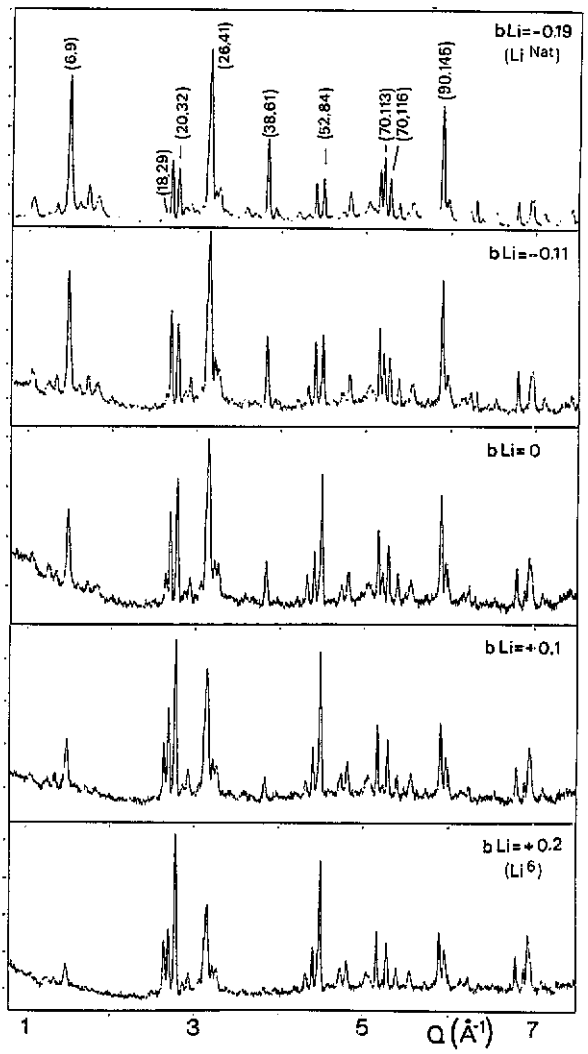

Figure 2. Neutron powder diffraction patterns as measured with samples of the ico-phase containing different $^6Li/^7Li$ isotopic mixtures; b(Li) is the corresponding scattering length. Contrast effects are clearly visible.

intensities were measured, corresponding to 56 independent reflections with intensities larger than three times their standard deviations. The typical ω-scan width of these reflections was found to be about three times as large as that of ordinary crystals of comparable size on the same apparatus. The single crystal neutron diffracted intensities were collected on the four-circle diffractometer D10 at the ILL, with a monochromatized neutron beam wavelength of $\lambda = 1.26$ Å. The icosahedral sample was a 5 mm size oriented dentrite, with typical ω-scan width of the reflections equal to 3°. In both x-ray and neutron single crystal data, absorption effects were neglected.

Using the indexing with six Miller pseudo-cubic indices $(h/h', k/k', l/l')$ [19] and the 6D hypercubic lattice constant $a = 7.15$ Å, both powder diffraction (with different contrast parameters) and four-circle diffraction peaks (x-rays and neutrons) were indexed by

$$Q_{\text{exp}} = Q_{\text{par}} = \frac{2\pi}{a\sqrt{2(2+\tau)}}(h + \tau h', k + \tau k', l + \tau l') \tag{1}$$

with an error of less than 10^{-3} Å^{-1}. The recorded reflections correspond to $(N, M) \leqslant (228, 368)$. They all belong to a primitive icosahedral Bravais lattice [19]. Incidentally, we have checked that the powder neutron diffraction pattern measured with the crystalline T1 phase (figure 2) was well interpreted with the structure proposed recently by Van Smaalen *et al* [22]. In a previously reported experiment [6], the partial pair distribution function has been measured, using the so-called direct space method [23]. The resulting information is going to be used hereafter.

4. Data analysis

As in classical crystallography, intensities of the powder diffraction peaks have to be corrected for Lorentz factor and absorption effects. The former is straightforward. The latter was carried out using the classical Paalman and Pings procedure. Neutron absorption is indeed tremendous with Li containing alloys, due to the very large absorption of the ^{6}Li isotope. Despite using special containers (cylinders with external diameter 10 mm and an empty core of diameter 8 mm) the transmission of the powder samples is typically only 25%, 18% and 10% for alloys containing ^{6}Li/^{7}Li mixtures with 50%, 75% and 100% of the absorbing ^{6}Li isotope, respectively.

The actual ^{6}Li/^{7}Li compositions have to be known for the accurate calculation of the partial structure factors. The nominal composition has to be checked carefully. This has been achieved by measuring the powder neutron diffraction patterns of LiF samples, whose structure is well specified, and then using the ^{6}Li/^{7}Li composition as an adjustable parameter to fit the data to the structure.

4.1. Aluminium/copper order

The AlLiCu quasicrystal is a ternary alloy. Three partial structure factors, with their amplitudes and phases, have to be determined if the structure is to be treated as a superimposed monoatomic system. Fortunately, the possibility of preparing samples with a 'zero scatterer' lithium ($Li^{(0)}$) yields some simplifications in as much as any ico-$AlCuLi^{(0)}$ sample actually behaves like a binary compound from the point of view of neutron diffraction. Thus, three such $Li^{(0)}$ bearing samples prepared with natural copper, ^{63}Cu and ^{65}Cu should lead to the determinations of Al/Cu atomic correlations. Actually

the powder neutron diffraction patterns corresponding to the extreme contrast obtained with ^{63}Cu and ^{65}Cu look very much the same for both alloys which means that Al/Cu order is very weak [6]. Thus, the (Al, Cu) atoms can now be treated as a single average species, say atom A, and the ico-phase as a pseudo-binary $A_{68}Li_{32}$ alloy whose partial structure factors may be obtained from Li isotopic substitution. Such a conclusion had been already reached in the pair distribution study [6].

4.2. Partial structure factors for A and Li atoms

The diffracted intensity at a given scattering vector $Q_{exp} = Q_{par}$ can be written

$$I(Q_{par}) = |F(Q_{par})|^2$$
$$= |b_A F_A(Q_{par}) + b_{Li} F_{Li}(Q_{par})|^2 \quad (2)$$

where b_A(constant) and b_{Li}(variable) stand for the neutron scattering length of the average A and Li atom, respectively. The F values are the corresponding partial structure factors. $I(Q_{par})$ are integrated intensities of the measured reflections. They are determined by a Guassian fit procedure as explained elsewhere in detail [1].

In the powder diffraction mode, the amplitudes $|Q_{par}|$ of Q_{par} are the only accessible scattering parameters. The measured intensities are then:

$$I(Q_{par}) = \sum_i \mu_i |F_i(Q_{par})|^2 \quad (3)$$

in which subscript i represents scanning of the different non-equivalent families of reflections showing up at the same Q and μ_i is the multiplicity of equivalent reflections in a given family i. Hereafter, peaks belonging to a single family of equivalent reflections will be referred to as 'simple reflections'. Their powder diffracted intensities are related to their single crystal diffracted intensity through their single multiplicity μ. The other reflections will be referred to as 'multiple reflections'.

As in regular crystallography, considering integrated intensities of the diffraction peaks somewhat disregards disorder. With the possible exception of the AlFeCu-like systems, almost all quasicrystals show some degree of phason disorder, manifested as broadening of the diffraction peaks. This is true for AlLiCu quasicrystals (figure 2) [23]. The approach taken in the present work forgets this aspect and relates to an ideal, unstrained AlLiCu quasicrystal.

Accordingly, and as already explained elsewhere [1, 24], equation (2) when applied to contrast variation data allows determination of amplitudes and phase differences of the partial structure factors (F_{Al}, F_{Li}). In the present case this has been carried out first with the simple reflections (25 of the measured ones) for both powder and single crystal data altogether. Then, x-ray and neutron four-circle data being renormalized with respect to each other, multiple reflections were treated the same way. Centro-symmetry of the structure (phase differences equal to 0 or π) was observed for the 66 measured independent reflections.

Degeneracy problems have been ruled out thanks to the single crystal data. This is a crucial point which certainly makes the structure specification more accurate in comparison with the case of AlMn quasicrystals [1, 2]. Reflections of the $(N, M) = (72, 116)$ families are illustrative of the point with almost zero intensity for one family and very strong intensity for the other.

5. Phase reconstruction and 6D periodic structure

Favourable circumstances have made phase reconstruction relatively easy for the AlMn quasicrystal [1, 2]. In the present case, the Q_{perp} dependences of the $|F_A|$ and $|F_{Li}|$ values (figure 3) are just clouds of points which do not suggest a clue to the (F_A, F_{Li}) signs. Consequently we had to work somewhat iteratively through successive steps of approximations.

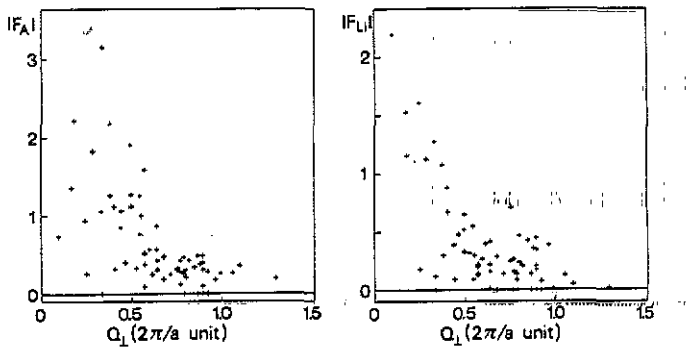

Figure 3. Q_{perp} dependences of the measured amplitudes of the partial structure factors. There is no evidence for simple behaviour, beyond a rough general decay at 'large' Q_{perp} values.

The starting point is of course the 66 independent reflections whose partial structure factors $|F_A|$ and $|F_{Li}|$, with their relative signs, have been obtained in section 4 of this paper.

A first easy step is to use the six-integer indexing of these reflections to Fourier transform $|F_A|^2$, $|F_{Li}|^2$ and $|F_A + F_{Li}|^2$ in a 6D direct space. The result is partial and total unweighted Patterson functions, repeating here a procedure first proposed by Gratias [3] and Cahn and co-workers [4]. Rational cross sections of these Patterson functions are shown in figure 5. From the density features visible in the figure and remembering that Patterson functions illustrate self-overlapping of the structure upon translation, it is easy to conclude that the $A3_{perp}$ volumes in the 6D cube are sited at vertex (OR) and mid-edge (ME) positions for A atoms and at body-centre (BC) positions for Li atoms. The partial structure factors should be written:

$$F_A(Q_6) = \frac{1}{V_6}\left[G_{OR}(Q_{perp}) + \sum_{i=1}^{6} G_{ME}^{(i)} \cos(Q_6 \cdot r_i)\right] \tag{4}$$

$$F_{Li}(Q_6) = \frac{1}{V_6} G_{BC}(Q_{perp}) \cos(Q_6 \cdot \delta). \tag{5}$$

G functions are the Fourier transforms of the $A3_{perp}$ volumes, V_6 is the volume of the 6D cube, $i = 1$–6 corresponds to the six different mid-edge positions and δ is the half-diagonal vector of the 6D cube.

As a first approximation, $F_{Li}(Q_6)$ can be calculated using equation (5) and a spherical $A3_{perp}$ (BC) whose volume is deduced from the Patterson functions (figure 5) along with

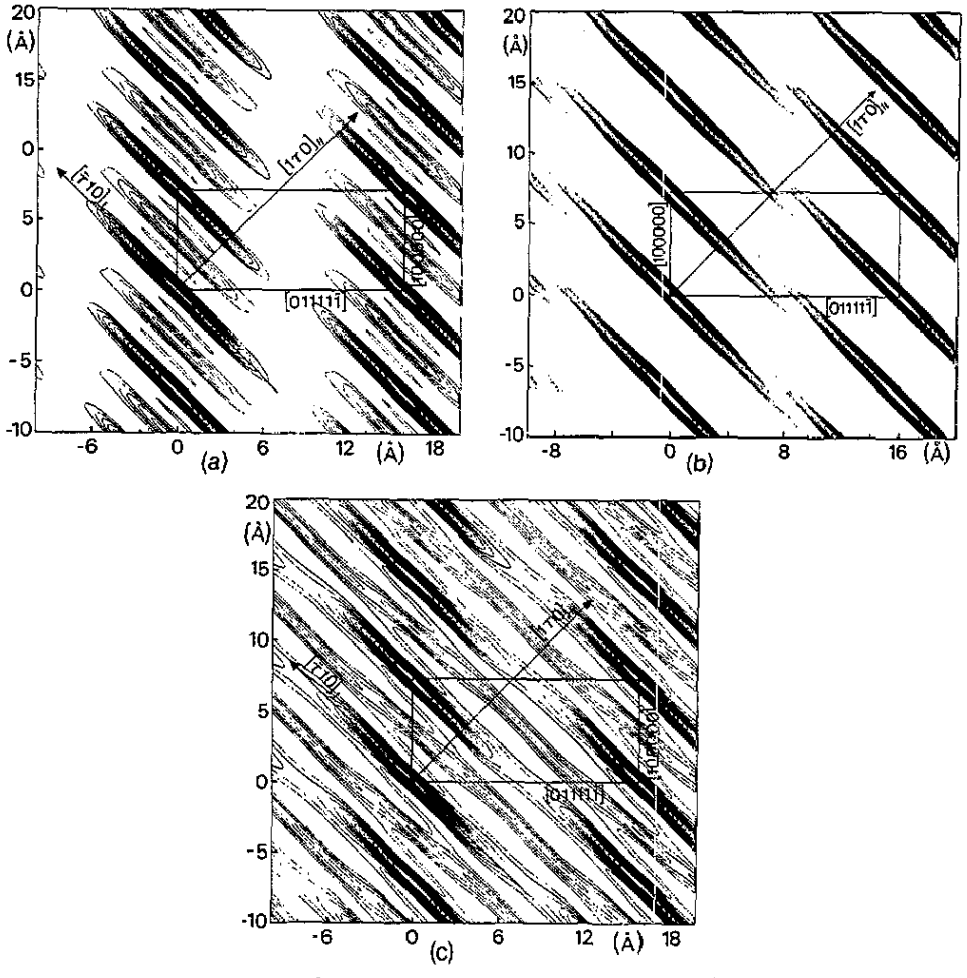

Figure 4. Patterson functions of the 6D periodic structure for (*a*) A, (*b*) Li and (*c*) A + Li atomic sites. The figures show a slice of the 6D space containing one perpendicular and one parallel fivefold axes.

composition and density data [21]. This 'equivalent' $A3_{perp}(BC)$ sphere has a radius of 8.54 Å.

The strongest experimental reflections are mainly influenced by size rather than shape details of $A3_{perp}$. Thus, it is reasonable to attribute signs to the strong experimental F_{Li} (typically for $Q_{perp} < 0.5$ in units of $2\pi/a$) identical to those of the spherical approximation. Now, signs of the corresponding F_A can also be derived since the F_A/F_{Li} relative signs have been experimentally determined. This gives about thirty independent reflections with the phases properly reconstructed for both F_A and F_{Li} experimental partial structure factors.

In the last step, the above thirty strongest pairs of partial structure factors are Fourier transformed in the 6D space. From the deduced partial density distribution, radii equal to 6.5 and 5.6 Å are obtained for the spherical equivalent $A3_{perp}$ volumes of the A atoms (vertex and mid-edge respectively). Again using equation (5), calculated values of F_A are used to attribute signs to the remaining experimental F_A and then F_{Li}; F_A and F_{Li}

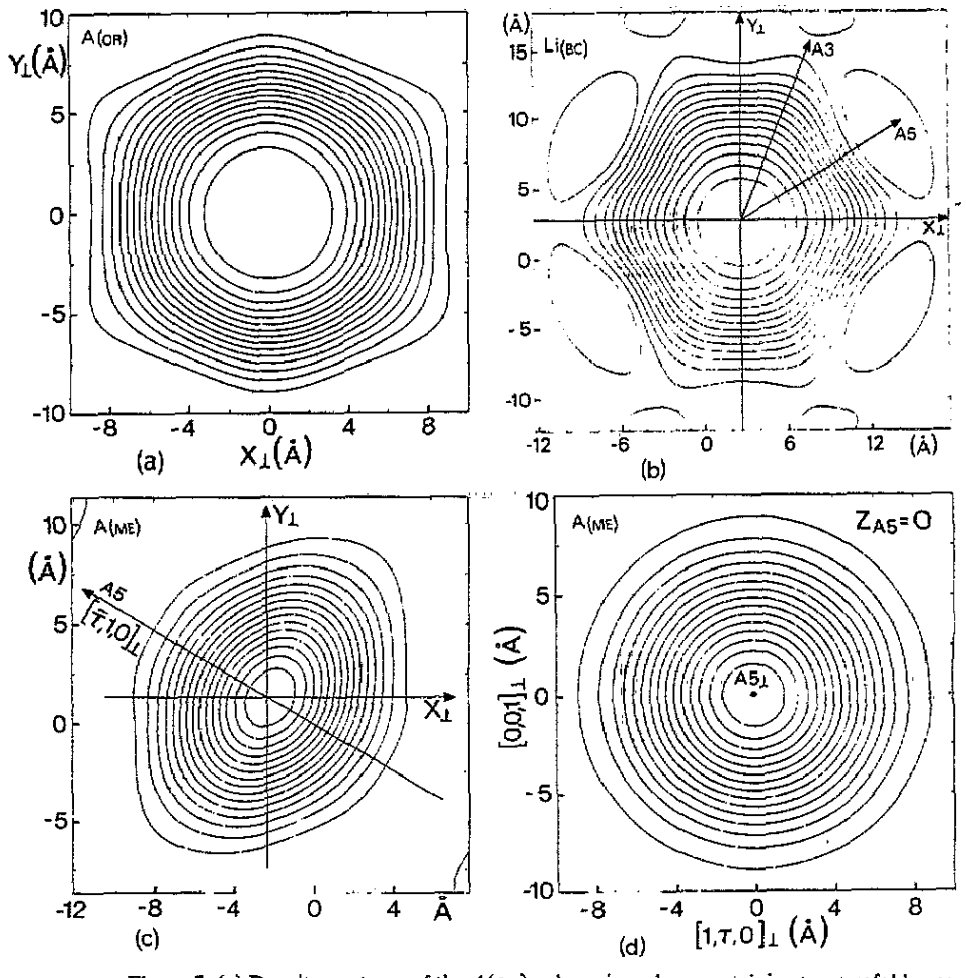

Figure 5. (*a*) Density contours of the A(OR) volume in a plane containing two twofold axes of the complementary space. (*b*) Same as in (*a*) but for the Li(BC) volume. (*c*, *d*) Same as in (*a*) but for two different cross sections of the A(ME) volume.

having their phases (0 or π) reconstructed unambiguously are given in table 1. The final 6D densities are illustrated in figure 5. The body-centre lithium volume is basically an 8 Å sphere with twenty added 'bubbles' along the threefold axes and twelve holes dug along the fivefold axes. The vertex A volume is also basically a 6.8 Å deformed sphere with added small volumes along the fivefold directions. Finally, the mid-edge A volume is more complicated, with fivefold axial symmetry and cross sections roughly circular in a plane perpendicular to its fivefold axis, roughly elliptical in a plane containing the fivefold axis and $(1, \tau, 0)_{perp}$ direction. The mid-edge volume has only a $\bar{5}m$ symmetry, the full icosahedral symmetry being recovered when the six mid-edge sites are considered altogether.

A 3D structure in our physical space can then be easily obtained by selecting the density part which has perpendicular coordinates equal to zero. Before doing that, the 6D structure is going to be improved by modelling.

Table 1. Experimental values of the partial structure factors F_A, F_{Li} with their phases reconstructed; Q_{par} and Q_{perp} are also given, along with multiplicity μ, indexing n_{6D} and (N, M) [19].

N	M	μ	Q_{par} (Å^{-1})	Q_{perp} ($2\pi/a$)	n_{6D}						F_A	F_{Li}
4	4	30	1.057	0.743	1	0	1	0	0	0	0.31	−0.25
6	9	20	1.481	0.398	0	1	1	0	0	1	1.12	−0.88
8	8	60	1.495	1.051	1	1	1	0	0	−1	−0.27	0.13
8	12	30	1.711	0.460	1	0	1	1	0	−1	−0.40	0.48
10	13	60	1.820	0.843	1	1	1	0	1	−1	−0.34	0.43
12	12	60	1.831	1.288	2	1	0	1	0	0	−0.20	−0.02
12	16	12	2.011	0.874	1	1	1	1	1	−1	−0.38	0.36
14	21	60	2.263	0.608	2	0	1	1	0	−1	0.25	−0.40
18	25	60	2.498	0.960	1	2	2	0	0	0	−0.18	−0.39
18	29	12	2.632	0.167	2	1	1	1	1	−1	−1.36	−1.53
20	28	120	2.640	0.987	1	2	2	0	1	0	−0.26	0.01
20	32	30	2.768	0.284	1	2	0	−1	2	0	1.83	1.13
22	33	120	2.837	0.762	2	1	1	2	0	−1	−0.29	0.00
24	36	60	2.963	0.796	2	1	1	2	1	−1	0.21	−0.47
24	36	20	2.963	0.796	2	2	0	0	2	0	0.31	−0.24
26	41	60	3.139	0.489	2	2	0	−1	2	0	1.91	−0.52
28	40	120	3.146	1.089	2	2	2	1	0	−1	−0.36	0.05
28	44	12	3.254	0.540	3	1	1	1	1	−1	−1.26	0.55
28	44	60	3.254	0.540	2	2	1	0	2	−1	0.77	−0.09
30	45	20	3.312	0.890	2	2	1	−1	2	−1	−0.49	0.45
30	45	60	3.312	0.890	3	0	1	2	0	−1	−0.31	0.18
30	45	60	3.312	0.890	2	2	1	1	2	−1	−0.10	−0.21
32	48	120	3.421	0.919	3	1	1	2	0	−1	−0.28	0.08
32	48	30	3.421	0.919	2	2	0	−2	2	0	0.00	0.00
34	53	60	3.575	0.671	3	1	1	2	1	−1	−0.19	0.29
36	56	120	3.676	0.709	2	2	3	0	0	1	0.25	−0.14
38	61	60	3.820	0.329	3	2	1	0	2	−1	1.06	−1.28
40	64	60	3.914	0.402	2	3	1	−1	2	1	−0.32	0.67
42	65	60	3.963	0.813	2	3	0	−2	2	0	0.43	0.21
46	73	60	4.185	0.565	3	1	2	2	1	−2	0.52	−0.13
46	73	60	4.185	0.565	2	3	0	−1	3	0	0.09	0.20
52	84	30	4.478	0.176	2	3	0	−2	3	0	2.22	1.16
56	88	60	4.601	0.764	3	3	0	−1	3	0	−0.12	−0.27
56	88	60	4.601	0.764	3	1	2	3	1	−2	−0.43	0.16
58	93	60	4.717	0.435	3	3	1	0	3	−1	−0.85	−0.39
60	96	20	4.794	0.492	3	3	1	−1	3	−1	−1.27	0.65
60	96	60	4.794	0.492	4	1	2	2	1	−2	1.12	0.33
62	97	60	4.834	0.861	3	3	0	−2	3	0	−0.49	0.14
62	97	120	4.834	0.861	3	4	1	−1	2	0	0.00	0.00
64	100	120	4.909	0.891	4	1	3	2	1	−1	−0.40	0.35
64	100	120	4.909	0.891	3	3	2	−1	3	0	0.00	0.00
66	105	60	5.017	0.633	4	2	2	1	2	−2	0.57	0.22
66	105	60	5.017	0.633	4	0	2	3	0	−2	0.87	0.01
68	108	120	5.090	0.673	4	2	3	2	0	−1	0.48	0.00
70	113	60	5.194	0.242	4	1	2	3	1	−2	0.94	−1.61
72	116	12	5.264	0.334	4	2	2	2	2	−2	3.15	0.12
72	116	60	5.264	0.334	4	3	1	0	3	−1	0.00	0.00
74	117	60	5.301	0.782	4	3	1	−1	3	−1	−0.29	−0.09
74	117	60	5.301	0.782	4	3	1	1	3	−1	−0.26	0.14
78	125	120	5.469	0.519	4	3	2	0	3	−1	0.33	−0.32

continued overleaf

Table 1. (*continued*)

N	M	μ	Q_{par} (Å^{-1})	Q_{perp} ($2\pi/a$)	n_{6D}						F_A	F_{Li}
80	128	30	5.535	0.568	2	4	0	−2	4	0	1.59	−0.22
80	128	120	5.535	0.568	4	1	3	3	1	−2	−0.38	0.14
90	145	60	5.886	0.373	3	4	0	−2	4	0	2.18	−1.08
92	148	120	5.948	0.438	4	1	3	4	0	−2	1.06	0.09
98	157	120	6.129	0.592	3	5	1	−2	3	1	−0.57	−0.27
100	160	60	6.189	0.635	4	4	1	0	4	−1	0.43	0.42
100	160	60	6.189	0.635	5	2	2	3	2	−2	0.32	0.16
100	160	30	6.189	0.635	4	0	3	4	0	−3	0.30	−0.01
102	165	20	6.275	0.094	4	4	4	1	1	1	0.74	−2.19
104	168	60	6.333	0.248	5	3	2	1	3	−2	−0.26	0.18
106	169	120	6.364	0.749	4	4	4	2	0	1	0.33	0.71
108	172	60	6.421	0.784	5	1	3	3	1	−3	−0.47	−0.09
108	172	60	6.421	0.784	4	4	1	−2	4	−1	0.00	0.00
108	172	120	6.421	0.784	0	3	5	0	−2	4	0.00	0.00
124	200	120	6.911	0.377	4	5	1	−2	4	0	1.26	0.30
130	209	60	7.068	0.548	4	5	2	−2	4	0	1.00	0.30

6. Modelling further. How and why

The partial structure factors being measured and their phases reconstructed, one may wonder why we are trying to model a structure when the density distributions, either in the 6D periodic lattice or in the 3D physical space, can be obtained by direct Fourier transforms of these partial structure factors. It is a reasonable approach which, however, may suffer some drawbacks. Most of these drawbacks have equivalents in classical crystallography where they have been overcome through model fitting procedures. A typical example is the so-called termination or truncation effect [25] which is even more dramatic in quasicrystallography because of the relatively restricted range of investigated Q_{perp} values. Some other difficulties, for instance parallel components of (or not flat) $A3_{perp}$ volumes [2], induce additional parameters which must be adjusted.

On the other hand, the experimental $A3_{perp}$ volumes may have features which are undesirable as they generate unphysically short atomic distances into the 3D structure. Thus, the $A3_{perp}$ have to be empirically 'retailored' for these too short distances to be removed. The principle of such a tailoring is illustrated in figure 6 which shows a rational cross section of a 6D hypercubic structure, with $A3_{perp}$ volumes on body-centre and mid-edge sites. Considering two of these volumes, labelled A(1) and A(2) in the figure, and the distance R_{par} between these volumes as measured along the physical axis of the cross section, the distance R_{par} is an actual atomic distance of the 3D structure if, and only if, a non-empty set of points is generated when A(2) is intersected by the R_{par} translated A(1). This is equivalent to considering the intersection of the projection of A(1) and A(2) into the $R3_{perp}$ space in which their centres are R_{perp} distant from each other. Thus, if the atomic distance R_{par} is to be avoided, holes of proper sizes and locations have to be dug out of A(1) or/and A(2) as exemplified in figure 6. A detailed report on such tailoring procedures has been published by Duneau and Oguey [26].

Scanning the distances between sites systematically results in a list of what has to be avoided for physical reasons. The strongest constraint corresponds to the distance between the $A3_{perp}$ volumes related to the body-centre Li sites and the mid-edge A

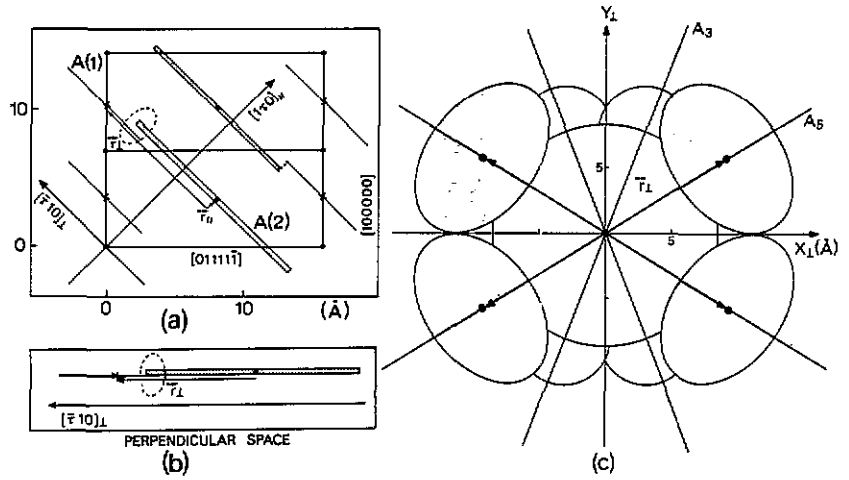

Figure 6. Fivefold axis slice (*a*) of the 6D space (schematic) showing 'overlapping' between BC and ME volumes A(1) and A(2). The short distance R_{par} will show up along a physical (par) fivefold axis because A(1) and A(2) have overlapping parts (in the broken loop) when projected onto the perp- fivefold axis (*b*). When looked at in a twofold axis plane of the perp-space (*c*) the A(1) volume is the white 'sphere' and the A(2) volumes are the grey ellipses. Clearly, parts of the white 'sphere' have to be dug out if overlapping has to be avoided.

sites, which is equal to 0.597 Å along a physical (par) fivefold axis (figure 6). This is unacceptably short and is removed by digging holes of the proper volume along the twelve fivefold axes of the BC volume. To restore the lost density, additional small volumes must be added where room is available. Figure 6 and the experimental results illustrated in figure 5 show that a clear possibility is around the twenty threefold axes.

The same analysis can be done for non-physical distances between ME–ME, OR–ME and ME–ME pairs of $A3_{perp}$ volumes. The whole procedure results in a set of $A3_{perp}$ models. The vertex A_{OR} volume is a sphere of 6.8 Å radius with an empty central hole of 2.3 Å radius; the mid-edge A_{ME} volume is an axial ellipse sited on a fivefold axis with geometrical size given by $a = 4.15$ Å and $b = c = 6.34$ Å; the body-centre Li_{BC} volume is a sphere of 8.5 Å radius with elliptical holes on fivefold axes (same a, b and c, as the ME site) and additional pieces of small spheres (radius 3.5 Å) on the threefold axes (figure 7).

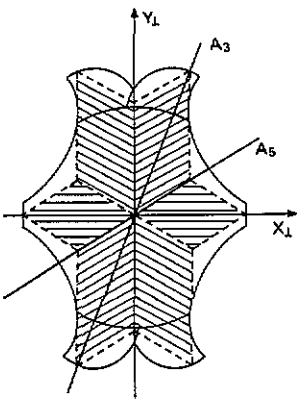

Figure 7. Cross section in the perpendicular space of the body centre volume as proposed in the model derived from diffraction data (full line). Compare with figure 5(*b*). Hatched areas within the broken lines show the stellation that generates a systematic decoration of the 3DPT threefold axes.

The direct cut of the above 6D structure by our physical 3D space generates atom positions into a cluster whose size is only limited by computer time. This is of course a somewhat brute force procedure but quite useful anyhow. We used it to build a spherical cluster and calculate pair distribution functions. These pair distribution functions are shown in figure 8 where they are compared with the one directly measured and reported in [6]. The result is quite satisfactory: all atomic distances and weight of the pairs are reasonably reproduced, without spurious unphysical short distances. In particular, the model fits positions and widths of the first distance peaks, which means that, contrary to the ico-AlMn structure [2], there are no parallel components in the $A3_{perp}$ volumes of the ico-AlCuLi system, at least down to a limit of about 0.05 Å.

Further validation of the model requires calculation of its Fourier components and comparing them to the diffraction data (single crystals and powders).

The adjustment of the model to data was attempted in a way reminiscent of classical crystallography with a scaling factor, plus a Debye–Waller factor (DW) for each of the three different $A3_{perp}$ volumes as free parameters. The relative Al/Cu compositions were also let free on the two A_{OR} and A_{ME} volumes in order to save a possible unobserved weak order to be compared with that existing in the crystalline R phase [27].

Residual factors (R, WR), χ^2 and DW are gathered in table 2. The DW factors are about twice those previously measured in the R phase [27] but still are reasonable values. The Al/Cu relative concentrations also have little influence on the fit qualities. The retained values obtained from x-ray data are $c(Al) = 0.879$ for the mid-edge sites and 0.716 for the vertex sites, instead of the 0.84 value that would correspond to total randomnness. Perpendicular Debye–Waller factors have no influence on the fit quality, suggesting that isotropic phason disorder is not a relevant property of the system.

The somewhat large value of the residual factors WR might be related to the weak peaks not being fitted correctly, because of misdefined details in the $A3_{perp}$ volumes. An

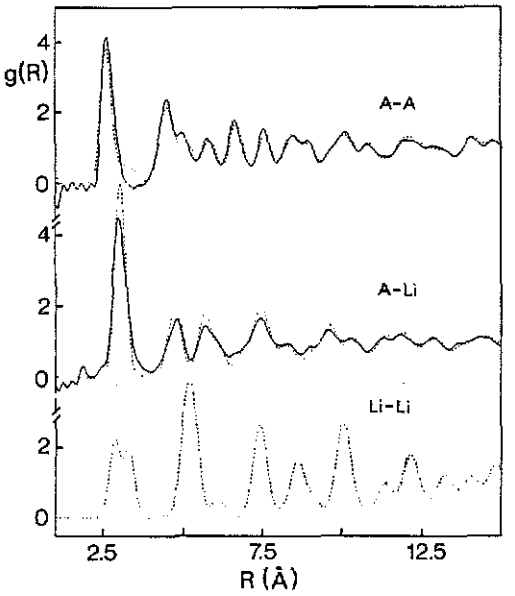

Figure 8. Partial pair distribution functions. Model (. . .) of the present work compared with experimental results from [6] (——).

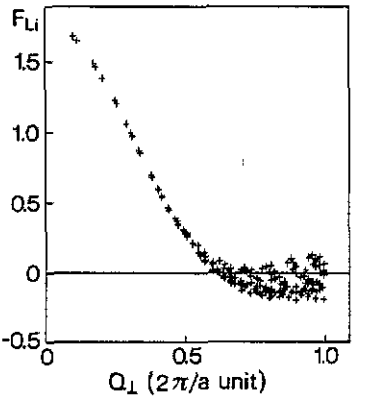

Figure 9. F_{Li} calculated with the present model. Differences with a spherical approximation show up mainly at relatively large Q_{perp} values.

Table 2. Residual factors, χ^2 and Debye–Waller factors as obtained from fitting the model to the single crystal data.

	R_F	R_F^2	wR	χ^2	$B_{(OR)}$	$B_{(ME)}$	$B_{(BC)}$
X-rays	0.08	0.08	0.17	24	2.22(6)	2.25(4)	2.6
Neutron	0.08	0.11	0.14	4	2.05(9)	1.91(6)	2.6

Table 3. Total structure factors as calculated, F_{model}, and measured F_{exp}, for the neutron single crystal data.

N	M	μ	Q_{par} (Å^{-1})	Q_{perp} ($2\pi/a$)	n_{6D}						F_{model}	F^2_{model}	F^2_{exp}	σ^2_{exp}
4	4	30	1.06	0.74	1	0	1	0	0	0	1.26	1.6	2.1	0.6
6	9	20	1.48	0.40	0	1	1	0	0	1	5.32	28.3	24.1	4.1
8	12	30	1.71	0.46	1	0	1	1	0	−1	−2.41	5.8	6.0	1.3
10	13	60	1.82	0.84	1	1	1	0	1	−1	−1.84	3.4	1.6	0.5
12	16	12	2.01	0.87	1	1	1	1	1	−1	−1.38	1.9	3.2	0.3
20	32	30	2.77	0.28	1	2	0	−1	2	0	5.05	25.5	22.7	2.8
26	41	60	3.14	0.49	2	2	0	−1	2	0	7.66	58.6	61.9	1.7
28	44	12	3.25	0.54	3	1	1	1	1	−1	−5.34	28.5	24.0	1.2
28	44	60	3.25	0.54	2	2	1	0	2	−1	2.49	6.2	6.8	1.0
30	45	20	3.31	0.89	2	2	1	−1	2	−1	−1.97	3.9	5.1	0.7
34	53	60	3.57	0.67	3	1	1	2	1	−1	−2.05	4.2	3.5	0.3
38	61	60	3.82	0.33	3	2	1	0	2	−1	5.12	26.2	27.1	1.5
40	64	60	3.91	0.40	3	2	1	1	2	−1	−1.94	3.8	4.7	0.6
46	73	60	4.19	0.57	3	1	2	2	1	−2	1.69	2.9	3.3	0.8
46	73	60	4.19	0.57	2	3	0	−1	3	0	0.77	0.6	3.2	0.8
52	84	30	4.48	0.17	2	3	0	−2	3	0	5.36	28.7	30.6	5.0
58	93	60	4.72	0.43	3	3	1	0	3	−1	−1.95	3.8	5.2	1.0
60	96	20	4.79	0.49	3	3	1	−1	3	−1	−5.22	27.3	23.5	2.7
60	96	60	4.79	0.49	4	1	2	2	1	−2	3.25	10.5	8.9	0.9
62	97	60	4.83	0.86	3	3	0	−2	3	0	−0.95	0.9	3.0	0.5
66	105	60	5.02	0.63	4	0	2	3	0	−2	2.77	7.7	7.1	2.2
70	113	60	5.19	0.24	4	1	2	3	1	−2	5.19	26.9	23.3	1.3
72	116	12	5.26	0.33	4	2	2	2	2	−2	9.80	96.1	101.6	3.0
72	116	60	5.26	0.33	4	3	1	0	3	−1	−1.46	2.1	3.2	0.8
78	125	120	5.47	0.52	4	3	2	0	3	−1	1.62	2.6	3.8	0.6
80	128	30	5.54	0.57	2	4	0	−2	4	0	5.01	25.1	26.4	2.1
90	145	60	5.89	0.37	3	4	0	−2	4	0	7.89	62.2	61.6	2.1
90	145	12	5.89	0.37	5	2	2	2	2	−2	7.44	55.4	62.5	3.0
92	148	120	5.95	0.44	4	1	3	4	0	−2	2.93	8.6	8.4	2.1
102	165	20	6.28	0.09	4	4	4	1	1	1	5.50	30.3	28.6	2.6
110	177	60	6.50	0.47	5	3	2	2	3	−2	1.97	3.9	5.7	2.1
122	197	60	6.86	0.30	5	4	3	1	3	−1	−1.56	2.4	3.9	1.1
124	200	120	6.91	0.38	5	4	4	2	1	0	3.19	10.2	8.8	1.1
130	209	60	7.07	0.55	5	4	4	2	2	0	3.44	11.9	15.5	1.0
154	249	60	7.71	0.20	6	4	4	2	2	−1	8.32	69.2	73.1	2.5
156	252	60	7.76	0.30	6	4	3	2	3	−2	3.17	10.1	8.4	1.0
156	252	20	7.76	0.30	5	5	1	−1	5	−1	−5.08	25.8	21.0	2.0
188	304	60	8.52	0.20	6	5	5	2	2	0	3.01	9.1	8.7	1.0
194	313	60	8.65	0.45	6	6	4	0	3	0	3.45	11.9	10.3	1.0
208	336	30	8.96	0.35	6	0	4	6	0	−4	5.13	26.3	23.5	3.0

illustration of the above statement is shown in figure 9 where the Fourier transform of the non-spherical BC(Li) volume appears as sensitive to shape details at large Q_{perp} reflection only.

For the powder diffraction data the R factors are of the order of 0.15 and χ^2 is about equal to 1–5 for the five contrasts. A quantitative comparison between model and data is presented in tables 3 and 4.

Table 4. Same as table 3 but for x-ray data.

N	M	μ	Q_{par} (Å^{-1})	Q_{perp} ($2\pi/a$)	n_{6D}						F_{model}	F^2_{model}	F^2_{exp}	σ^2_{exp}
4	4	30	1.06	0.74	1	0	1	0	0	0	1.31	1.7	1.9	0.1
6	9	20	1.48	0.40	0	1	1	0	0	1	5.10	26.0	26.1	0.5
8	8	60	1.50	1.05	1	1	1	0	0	−1	−0.69	0.5	2.0	0.2
8	12	30	1.71	0.46	1	0	1	1	0	−1	−1.61	2.6	2.7	0.1
10	13	60	1.82	0.84	1	1	1	0	1	−1	−1.88	3.5	2.2	0.2
12	12	60	1.83	1.29	2	1	0	1	0	0	−0.55	0.3	1.2	0.1
12	16	12	2.01	0.87	1	1	1	1	1	−1	−1.49	2.2	2.8	0.1
14	21	60	2.26	0.61	2	0	1	1	0	−1	1.07	1.1	0.9	0.2
18	25	60	2.50	0.96	1	2	2	0	0	0	−0.97	0.9	1.3	0.1
18	29	12	2.63	0.17	2	1	1	1	1	−1	−6.10	37.2	39.7	0.7
20	28	120	2.64	0.99	1	2	2	0	1	0	−1.43	2.0	1.5	0.2
20	32	30	2.77	0.28	1	2	0	−1	2	0	9.91	98.2	95.6	1.6
22	33	120	2.84	0.76	2	1	1	2	0	−1	−1.08	1.2	1.1	0.1
24	36	60	2.96	0.80	2	1	1	2	1	−1	0.32	0.1	0.4	0.1
24	36	20	2.96	0.80	2	2	0	0	2	0	1.13	1.3	1.5	0.1
26	41	60	3.14	0.49	2	2	0	−1	2	0	7.84	61.5	60.9	1.1
28	40	120	3.15	1.09	2	2	2	1	0	−1	−1.24	1.5	2.3	0.2
28	44	12	3.25	0.54	3	1	1	1	1	−1	−5.29	27.9	25.1	0.5
28	44	60	3.25	0.54	2	2	1	0	2	−1	3.33	11.1	10.3	0.3
30	45	20	3.31	0.89	2	2	1	−1	2	−1	−1.62	2.6	3.1	0.1
30	45	60	3.31	0.89	3	0	1	2	0	−1	−1.66	2.8	1.4	0.1
30	45	60	3.31	0.89	2	2	1	1	2	−1	−0.16	0.0	0.3	0.1
32	48	120	3.42	0.92	3	1	1	2	0	−1	−0.99	1.0	1.2	0.1
34	53	60	3.57	0.67	3	1	1	2	1	−1	−1.94	3.8	3.3	0.1
36	56	120	3.68	0.71	2	2	3	0	0	1	0.88	0.8	0.8	0.1
38	61	60	3.82	0.33	3	2	1	0	2	−1	3.11	9.7	9.6	0.3
46	73	60	4.19	0.57	3	1	2	2	1	−2	1.50	2.3	3.2	0.1
46	73	60	4.19	0.57	2	3	0	−1	3	0	0.45	0.2	0.2	0.1
52	84	30	4.48	0.17	2	3	0	−2	3	0	8.50	72.3	78.8	1.3
56	88	60	4.60	0.76	3	3	0	−1	3	0	0.05	0.0	0.3	0.1
56	88	60	4.60	0.76	3	1	2	3	1	−2	−1.47	2.2	1.8	0.1
58	93	60	4.72	0.43	3	3	1	0	3	−1	−2.67	7.1	7.9	0.3
60	96	20	4.79	0.49	3	3	1	−1	3	−1	−4.07	16.5	14.2	0.4
60	96	60	4.79	0.49	4	1	2	2	1	−2	3.61	13.0	14.2	0.4
62	97	60	4.83	0.86	3	3	0	−2	3	0	−1.02	1.0	2.2	0.1
64	100	120	4.91	0.89	4	1	3	2	1	−1	−0.81	0.7	1.2	0.1
66	105	60	5.02	0.63	4	2	2	1	2	−2	1.93	3.7	3.5	0.2
66	105	60	5.02	0.63	4	0	2	3	0	−2	2.36	5.6	7.2	0.3
68	108	120	5.09	0.67	4	2	3	2	0	−1	1.35	1.8	2.1	0.1
70	113	60	5.19	0.24	4	1	2	3	1	−2	2.35	5.5	5.1	0.2
72	116	12	5.26	0.33	4	2	2	2	2	−2	9.81	96.3	100.0	1.6
74	117	60	5.30	0.78	4	3	1	−1	3	−1	−0.65	0.4	0.8	0.1
74	117	60	5.30	0.78	4	3	1	1	3	−1	−1.22	1.5	0.5	0.1
78	125	120	5.47	0.52	4	3	2	0	3	−1	1.04	1.1	1.6	0.1

Table 4. (*continued*)

N	M	μ	Q_{par} (Å^{-1})	Q_{perp} ($2\pi/a$)	n_{6D}						F_{model}	F^2_{model}	F^2_{exp}	σ^2_{exp}
80	128	30	5.54	0.57	2	4	0	−2	4	0	4.19	17.6	18.5	0.5
80	128	120	5.54	0.57	4	1	3	3	1	−2	−0.72	0.5	1.0	0.1
90	145	60	5.89	0.37	3	4	0	−2	4	0	5.07	25.8	27.4	0.6
92	148	120	5.95	0.44	4	1	3	4	0	−2	2.88	8.3	7.7	0.3
98	157	120	6.13	0.59	3	5	1	−2	3	1	−1.56	2.4	2.2	0.2
100	160	60	6.19	0.63	4	4	1	0	4	−1	1.31	1.7	1.4	0.1
100	160	60	6.19	0.63	5	2	2	3	2	−2	0.89	0.8	0.7	0.1
100	160	30	6.19	0.63	4	0	3	4	0	−3	0.33	0.1	0.5	0.1
102	165	20	6.28	0.09	4	4	4	1	1	1	2.01	4.0	2.7	0.2
104	168	60	6.33	0.25	5	3	2	1	3	−2	0.48	0.2	0.3	0.1
106	169	120	6.36	0.75	4	4	4	2	0	1	0.87	0.8	1.0	0.1
108	172	60	6.42	0.78	5	1	3	3	1	−3	−0.97	0.9	1.2	0.2

7. Atomic structure of the AlCuLi quasicrystal in 3D physical space

As already stated, the straightforward method to obtain atomic positions is to generate their three coordinates as intersections of the 6D periodic structure by our physical space. An alternative way of getting these coordinates is to Fourier transform the partial structure factors (with their phases) directly in the 3D space as explained in [28]. Both methods give the same results as exemplified in figure 10. According to observations made on pair distribution functions [6], a more physical description may be attempted within a comparison of the ico-phase structure with that of the cubic R-phase [27]. The structure of the R-phase as determined by Audier *et al* [27] belongs to the *Im*3 (BCC) space group with a lattice parameter of 13.9056 Å. The Al, Cu, Li atoms are distributed over shells around the origin. The set of successive polyhedra from centre to surface forms the so-called 'Samson's complex' which contains 104 atoms. The structure of R-Al_5CuLi_3 can then be described as a CsCl-type packing of distorted Samson polyhedra linked in two ways.

(i) Along edges of the cubic cell by sharing two aluminium atoms (site 12e).

(ii) Along the eight body diagonals of the cube by sharing a common hexagonal face of the polyhedra (site 48h). The remaining lithium atoms (site 12e) are found in the interstices formed within the Samson polyhedron packing. They cap the pentagonal faces of a truncated icosahedron. The site 12e (Li atoms) are located at 24 of the 32 vertices of a 'large' rhombic triacontahedron of radius $r = 8.18$ Å. The eight remaining vertices coincide with the Li in 16f sites already considered in the formation of the underlying dodecahedral shell. The distorted truncated icosahedra have not a perfect icosahedral symmetry which would have forced the atoms in 48h sites to emerge at the surface of the outer triacontahedral atomic shell. There are two triacontahedral shells (so-called 'small' and 'large' heretofore) with diameters in a ratio practically equal to the golden mean τ. All the Al/Cu atoms are in the shells of a 'soccer ball' (small and large icosahedron plus external shell of the truncated icosahedron) while Li atoms are on the external shell of the large and small triacontahedra.

The conditions to be fulfilled by the $A3_{perp}$ volumes for generating a given type of atomic clusters in the cut procedure have been analysed by several authors [15, 26, 29].

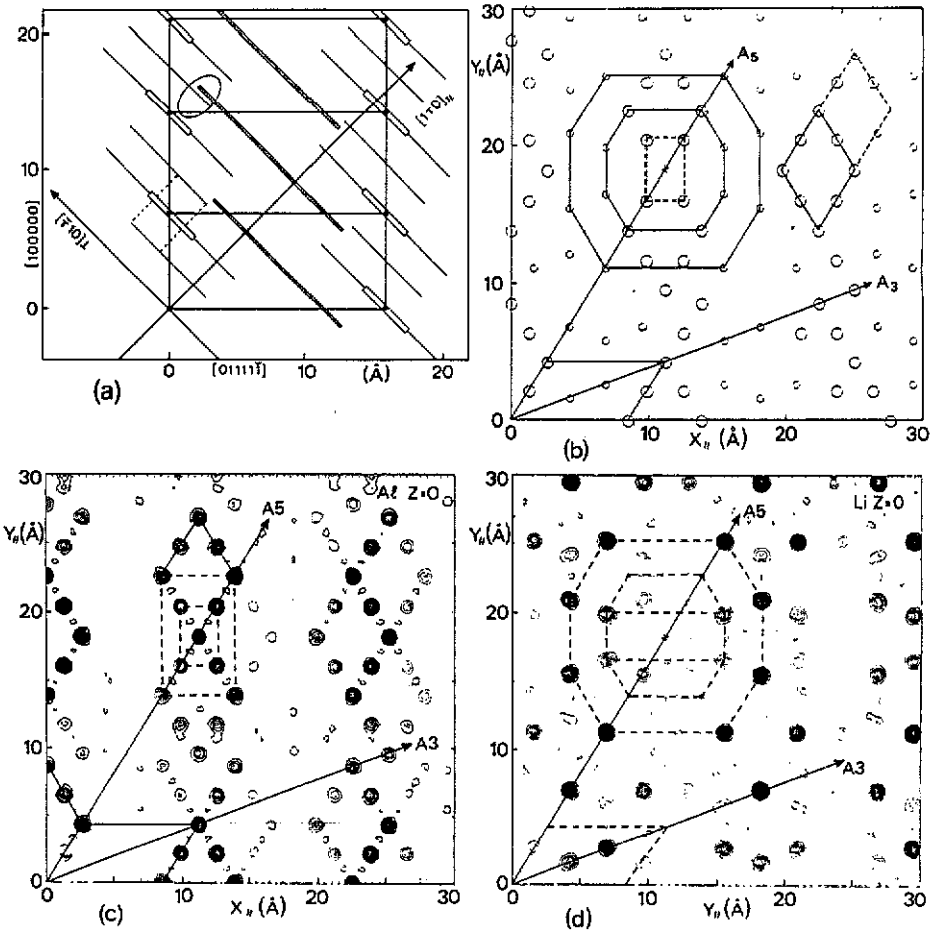

Figure 10. Part (*a*) of the figure shows a schematic of a fivefold axis slice of the 6D model structure, with cross sections of the vertex, mid-edge and body-centre volumes. We have highlighted an example of a distance which is too short in the loop, as detailed in figure 6. The dashed rectangle shows the acceptance domain for ME–ME distances through the central hole of the vertex volume. The physical fivefold axis $[1\tau 0]_{par}$ crosses the $A3_{perp}$ volumes at 3D atomic positions as shown in figure 10(*b*) which presents a slice of the 3D atomic density as deduced from the model (large and small circles are A and Li atoms, respectively). Cross sections of small (large) triacontahedra and rhombohedral tiles are also shown. The model density (10(*b*)) compares quite well with the corresponding density map as directly obtained from FT of the experimental F_A (10(*c*)) and F_{Li} (10(*d*)).

The basic principles are very similar to those used in section 6 in the procedure of identification and elimination of the too short atomic distances and can be worked out in the complementary (perp) space. A cluster is completely defined when atomic bonds between centre-to-shell atoms are identified. For instance, the presence of icosahedral clusters in the 3D structure will correspond to the existence of families of twelve equal atomic distances converging along fivefold axes. In the 6D structure, this is equivalent to say that a given $A3_{perp}$ volume has twelve neighbours distributed along pertinent directions and in such a way that the cut procedure generates the proper atomic pairs.

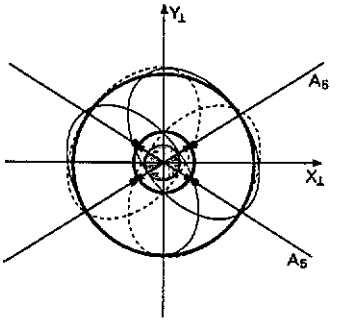

Figure 11. Schematic view of the definition of the acceptance domain for small icosahedra as the common region between a vertex and twelve neighbour mid-edge $A3_{perp}$ when projected into the perpendicular space. This is a 2D cross section.

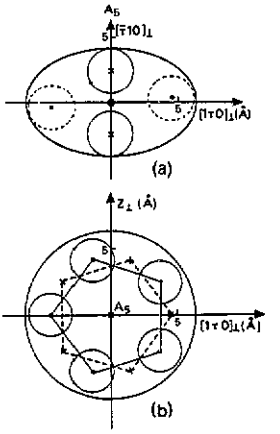

Figure 12. Representation of the acceptance domains for small icosahedra (full line circles) and for soccer-balls (broken line circles) when projected on the mid-edge volume. (*a*) is a cross section containing the fivefold axis of the ellipse; (*b*) is a cross section perpendicular to the fivefold axis with two pentagons (size 4.25 Å) of acceptance domains at 0.27 Å on each side of the ellipse equatorial plane.

In the 6D structure model, one vertex A_{OR} volume is surrounded by twelve mid-edge A_{ME} volumes. The cut procedure generates A–A distances equal to 2.528 Å if the projected of the A_{OR} and A_{ME} into the perpendicular space have parts of their volumes in common. This is visible in figure 10(*a*). The twelve projected A_{ME} having a small common volume (figure 11), roughly a sphere of 1.65 Å radius, indicates that small icosahedra of A atoms will be found in the 3D atomic structure. This common volume is called the acceptance domain and gives, in particular, the occurrence rate of the corresponding clusters into the structure. As shown in figures 10(*a*), 11 and 12 the acceptance domains corresponding to the external shell of the 'soccer balls' are identical to that of a small icosahedra; both correspond to the common volume in perpendicular space of the 12 A_{ME} adjacent to a given A_{OR}. More generally it can be demonstrated that all the shells present in a soccer ball have the same acceptance domain though coming from different association of $A3_{perp}$ volumes.

Thus, as summarized in table 5, all the atomic shells typical of the R-phase structure were also found in the ico-phase, up to the so-called large triacontahedron. The cross sections at $z = 0$ of the 3D density distribution presented in figure 13 show also very clearly the presence of the two (small and large) triacontahedra and the other icosahedral clusters. The acceptance domains may be finely facetted but the spherical approximation is sufficient to provide at least an estimate of the proportion of Al/Cu atoms within the soccer ball clusters. This proportion is found equal to only 28%, while soccer balls contain all the atoms of the R-phase structure. These soccer balls are weakly connected only along threefold axes by having hexagonal faces in common; this is at variance with the (distorted) soccer balls of the R-phase which share additionally Al atoms along twofold axes. The drawing shown in figure 12 illustrates that the acceptance domain of the soccer balls cannot be enlarged significantly; the limitation comes from the size of

Table 5. Atomic distances and atomic shells showing up in the ico-phase model, compared with the R-phase.

Atoms	Polyhedron	n_{6D} [18]						μ	Site	R_{perp} (Å)	R_{par} (Å)	R-phase
Al–Cu	small icosahedron	0	0.5	0	0	0	0	12(A5)	ME	2.528	2.528	2.51
Li	small dodecahedron	0.5	0.5	−0.5	0.5	0.5	0.5	20(A3)	BC	7.45	4.604	4.51
Al–Cu	triacon–icosahedron	0	1	0.	0	0	0	12(A5)	OR	5.056	5.056	5.046
Al–Cu	soccer ball	0	1	0	0	0.5	0	60(MIR)	ME	4.53	6.587	6.603
												7.081
Li	dodecahedron	0.5	0.5	0.5	−0.5	−0.5	−0.5	20(A3)	BC	4.604	7.449	7.47
	large triacon											7.53
Li	icosahedron	0.5	0.5	0.5	−0.5	0.5	0.5	12(A5)	BC	3.125	8.18	8.18

the equatorial circle of the ellipsoidal A_{ME} volume which, in turn, cannot be larger if too short A_{ME}–Li_{BC} distances have to be avoided (figure 6). On the contrary, the acceptance domain for the small icosahedra and small triacontahedra could be enlarged without too much inconvenience by elongating the ellipsoidal A_{ME} volume (see again figures 6 and 12) in its fivefold directions.

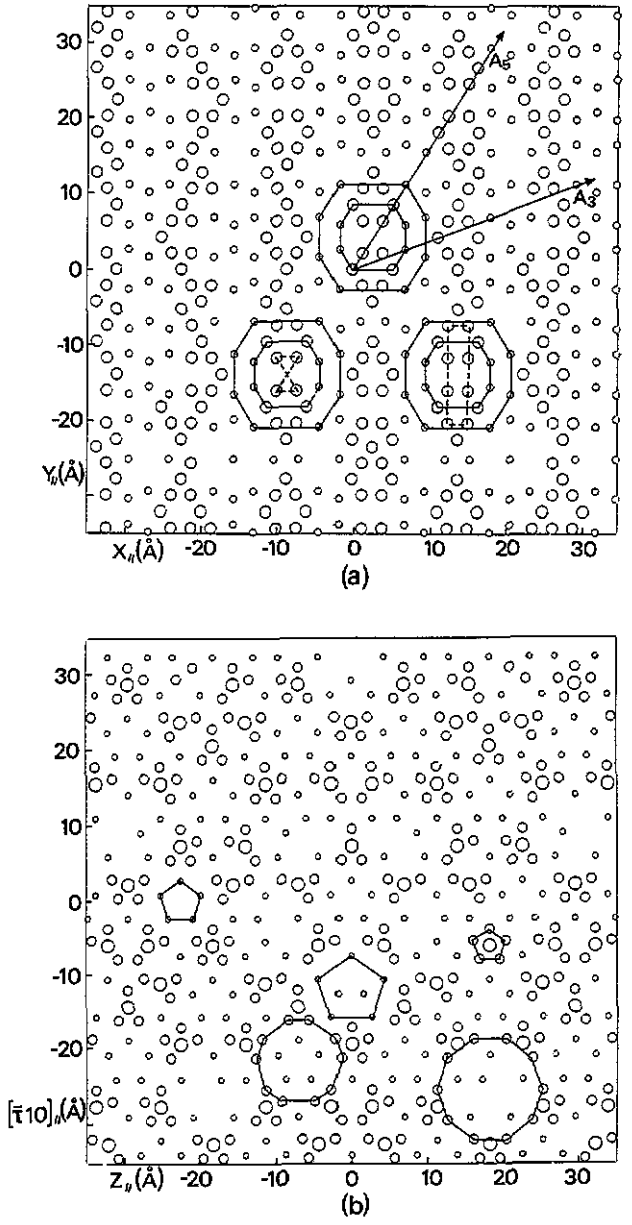

Figure 13. Cross sections of the 3D atomic density corresponding to twofold (*a*) and fivefold (*b*) planes. Traces of the various icosahedral clusters are visible (A = large and medium circles; Li = small circles) as three planes composite and soccer balls (large decagons) in the fivefold map and triacontahedra in the twofold map.

From a model previously proposed by Audier and Guyot [30], it is known that an acceptance domain defined by a τ^3-deflated triacontahedron (edges equal to $5.05/\tau^3$ Å and volume equivalent to a sphere of 1.7 Å radius) corresponds to a τ^3 inflated three-dimensional Penrose tiling of the space (edges of $5.505 \times \tau^3$ Å). This demonstrates that, in the present determined structures of the AlCuLi quasicrystals, most of the large triacontahedra containing the soccer balls are on the vertices of a τ^3-inflated 3DPT. As already stated these clusters would contain about 28% of the Al/Cu atoms and 7% of the Li atoms. As it is not possible to increase the acceptance volume for these large triacontahedra, it is sensible to try to complete the structure with small triacontahedra. Providing a proper acceptance domain, most of them would indeed be on the face diagonals of the tiles of the τ^3-inflated 3DPT and also on the prolate triad axis. But the decoration would not be identical from tile to tile. Thus, even in its τ^3-inflated modification, a 3DPT may not be a good approach to this quasicrystal structure. Looking for icosahedral clusters of the sort existing in the R-phase is of course a little restrictive. The rather small fraction of atoms included in the soccer balls is a measure of the degree of similarity between R- and ico-phases and suggests that other types of clusters must be involved in the structure of the ico-phase.

Incidentally, it is also interesting to confront the structure proposed in the present work with models in which the atomic decoration is made directly on the elementary Penrose lattice (edges of 5.05 Å), as proposed for instance by Van Smaalen and co-workers [31, 32]. On the selected cross sections of the 3D density shown in figures 10 and 13, images of rhombohedral tiles are indeed visible. The Al atoms generated by the cut of the 6D vertex volume are sited on 3D vertex of the 3DPT, but due to the central hole of the A_{OR} volume and its external size, some vertices are unoccupied. The Al atoms generated by cut of the mid-edge volume are also in mid-edge positions in the 3DPT, but again with partial occupancy only. The Li atoms are generated mostly on the triad axis of the prolate rhombohedra, in a $\tau/1/\tau$ partition, but also occasionally at edge positions at 1.93 Å of unoccupied vertices. Thus, when the structure is assumed to be 3DPT-like, the decoration of the tiles is not unique.

In their attempts to describe the structure in terms of a 3DPT with a single type of tile decoration, Van Smaalen [31] and Elswijk *et al* [32] had to inject a nonphysical AlCu/Li disorder into the structure; the difficulties that they encountered might be good evidence of how much a 3DPT is non-physical and not suitable for specifying quasicrystal structures. The 6D structure as proposed by Van Smaalen [33], based on x-ray single crystal data and symmetry conditions for the possible $A3_{perp}$ volumes, is also a primitive hypercubic lattice with atomic volumes at vertex and mid-edge positions for AlCu atoms but the body centre volume was not observed because x-rays are not sensitive to lithium atoms.

Henley and Elser [34] had also previously proposed a tiling model with three different tiles, namely the classical prolate and oblate rhombohedra plus a rhombic dodecahedron. The proposed decoration had something of what we have observed: Al/Cu atoms on vertex and mid-edge positions; Li atoms on edges of prolates inside the dodecahedron at 1.93 Å of their empty centre.

Qiu and Jaric [35] have recently reported on a new method to reconstruct the phases of the measured structure factors. These phases were considered as parameters to be determined by the best fit between a hypothetical rational approximate of the quasicrystal and real crystal x-ray data (present work and [27]). They have reached an interesting specification of the Al/Cu 6D substructure (Li not visible with x-rays). Their $A3_{perp}$ volumes are very similar, with differences in details, to those reported in the

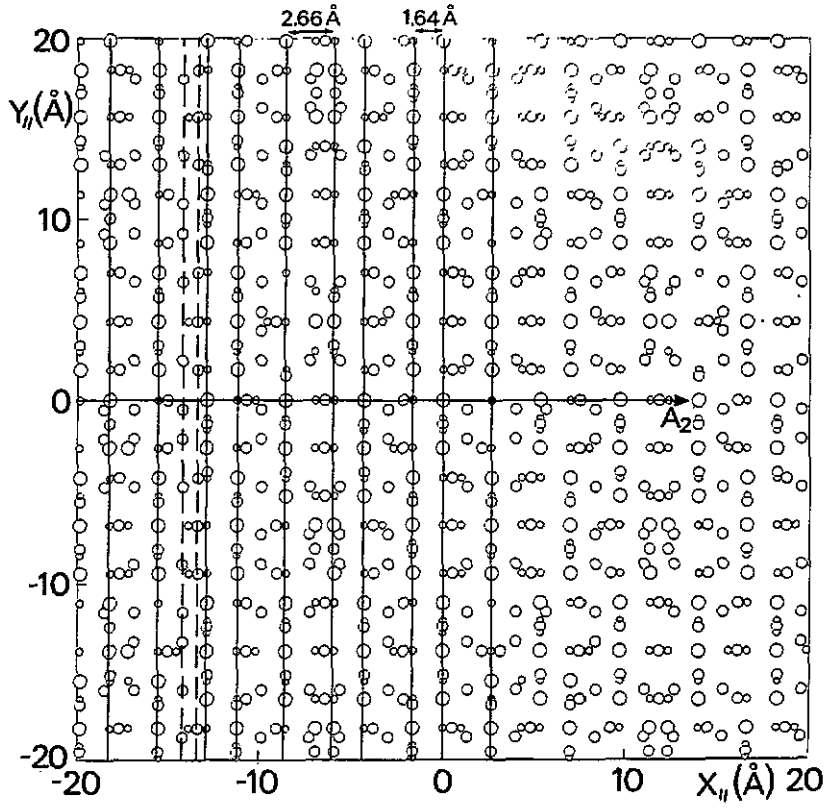

Figure 14. Structure of the 3D density as described by families of twofold atomic planes as obtained from projections of atom positions contained into a 40 × 40 × 40 Å cube. A_{OR}, A_{ME} and Li_{BC} atoms are shown as large, medium and small open circles, respectively. Solid and dashed lines exemplify more and less dense planes in the twofold family, respectively.

present work. In particular, the more elongated shape of the mid-edge volume in the direction of fivefold axes increases the acceptance domains for small triacontahedra (≈2.7 Å radius instead of 1.8 Å in term of spherical equivalence).

Finally, a last alternative way of visualizing the 3D structure may be a description in terms of atomic planes. Such a description can be obtained rather easily from the appropriate physical cut of the 6D periodic structure. The point is exemplified in figure 14 showing a family of atomic 'planes' perpendicular to a twofold direction. Two different average repetition distances, namely 1.643 and 2.658 Å in a ratio of $1/\tau$, and arranged into a Fibonnacci sequence, are observed. Their average d-spacing corresponds to one of the strongest diffraction peak, i.e. $(N, M) = (20, 32)$. The twofold planes are also the most dense and more distant from each other (as compared with threefold or fivefold plane families). They are formed by two different types of layers: (i) dense layers with A atoms (originating from both vertex and mid-edge volumes) and Li atoms; (ii) less occupied layers with either A or Li atoms alone. Threefold or fivefold planes never contain the three types of atoms simultaneously. Such a description is reminiscent of a property of the simple 3DPT in which planes of atoms and columnar structures have been pointed out by Duneau and Katz [15]. Finally, the structure as described in terms of atomic plane families allows us to understand the observed morphology of the single

(quasi)crystal AlCuLi, along rules analogous to those of classical crystal growth. Indeed, the triacontahedral single grains which have been obtained, have facets perpendicular to twofold axes and edges along fivefold axes, the most dense atomic planes and rows. Accordingly it may be conjectured that AlSiMn quasicrystals tend to grow into dodecahedral or/and icosidodecahedral grains because of a different atomic decoration which produces highest density in fivefold or threefold atomic planes [1, 2].

8. Conclusions

A detailed neutron and x-ray diffraction study of the AlCuLi quasicrystal has been completed. The association of contrast variation effects, thanks to both Cu and Li isotopic substitutions, and single crystal investigations allows the best experimental determination of partial structure factors, with their amplitudes and phases. The procedure for data analysis, though being worked out in 6D space, is reminiscent of early age classical crystallography: Patterson functions are used to suggest a density model which is further refined up to convergency with diffraction data.

The physical 3D structure has then been generated by a proper cut of the high-dimensional description. Atom positions can then be simply listed for further use as such or analysed in terms of atomic plane families, statistics of atomic identified clusters, 3DPT (inflated or not). Forcing the structure into the 3DPT with 5.05 Å edges results in unphysical AlCu/Li disorder [31, 32], or non-unique decoration of the tiles. Even the τ^3-inflated 3DPT suffer the same drawbacks though to a lesser extent. This may not be very surprising and it has been known for several years [36] that there are structures which are neither decorations of 3DPTs nor strict projection from six dimensions which are nevertheless icosahedral quasicrystals (random tiling models).

However, when the latter applies properly, and assuming that the $A3_{perp}$ volumes of the 6D structure can be designed in detail, complete information about atomic positions remains contained in this higher space periodic description, within the usual very condensed aspect of the decorated unit cell. Unfortunately, we are still ignoring how to project this information (if possible!) into our physical space. In the cut procedure, part of the structural information is unavoidably lost and hidden in six dimensions, resulting in limitations of size and type of clusters or atomic planes, unsatisfactory 3DPT etc. As such, the 3D structure may be very useful anyhow and it permits progress into the understanding of quasicrystals.

Acknowledgments

The authors are very grateful to Michel Duneau for very fruitful discussions. Samples have been prepared at the Research Centre of Pechiney (Voreppe, France); ILL has also to be acknowledged for generous allocation of beamtime. Gernot Heger and Jean Pannetier brought definitive contributions to this work, in particular by participating to x-ray and neutron data collection.

References

[1] Janot C, De Boissieu M, Dubois J M and Pannetier J 1989 *J. Phys.: Condens. Matter* **1** 1029
[2] De Boissieu M, Janot C and Dubois J M 1990 *J. Phys.: Condens. Matter* **2** 2499

[3] Gratias D 1988 *Quasicrystalline Materials* ed C Janot and J M Dubois (Singapore: World Scientific) p 83
[4] Cahn J W, Gratias D and Mozer B 1988 *J. Physique* **49** 1225; 1988 *Phys. Rev.* B **38** 1638; 1988 *Phys. Rev.* B **38** 1643
[5] Shechtman D, Blech I, Gratias D and Cahn J W 1984 *Phys. Rev. Lett.* **53** 1951
[6] De Boissieu M, Janot C, Dubois J M, Audier M and Dubost B 1989 *J. Physique* **50** 1689
[7] Sainfort P, Dubost B and Dubus A 1985 *CR Acad. Sci.* **301** 689
[8] Dubost B, Lang J M, Tanaka M, Sainfort P and Audier M 1986 *Nature* **324** 48
[9] Gayle F W 1987 *J. Mater. Res.* **2** 1
[10] Kortan A R, Chen H S and Waszczak J V 1987 *J. Mater. Res.* **2** 351
[11] Parsey J M, Chen H S, Kortan A R, Thiel F A, Miller A E and Farrow R C 1988 *J. Mater. Res.* **3** 233
[12] Elsavijk H B and De Hosson J T M 1988 *Phys. Rev.* B **38** 1681
[13] Van Smaallen S, Bronsveld P and De Boer J L 1987 *Solid State Commun.* **63** 751
[14] Denoyer F, Heger G, Lambert M, Lang J M and Sainfort P 1987 *J. Physique* **48** 1357
[15] Duneau M and Katz A 1985 *Phys. Rev. Lett.* **54** 2688
[16] Kalugin P A, Pitayev A Y and Levitov L S 1985 *Sov. Phys.–JETP Lett.* **41** 119
[17] Elser V 1985 *Phys. Rev.* B **32** 4892
[18] Bak P 1985 *Phys. Rev. Lett.* **54** 1517
Janssen T 1988 *Phys. Rep.* **168** 55
[19] Cahn J W, Shechtman D and Gratias D 1986 *J. Mater. Res.* **1** 13
[20] Levitov L S and Rhyner J 1988 *J. Physique* **49** 1835
[21] Dubost B, Collinet C and Ansara I 1988 *Quasicrystalline Materials* ed C Janot and J M Dubois (Singapore: World Scientific) pp 39–52
[22] Van Smaalen S, Meetsma A, De Boer J L and Bronsveld P H 1989 *Preprint*
[23] Heiney P A, Bancel P A, Horn P M, Jordan J L, Laplaca S, Angilello J and Gayle F W 1987 *Science* **238** 661
[24] Roth M, Lewit-Bentley A and Bentley G A 1984 *J. Appl. Crystallogr.* **17** 77
[25] De Boissieu M, Janot C and Dubois J M 1988 *Eur. Phys. Lett.* **7** 593
[26] Duneau M and Oguey C 1989 *J. Physique* **50** 135
[27] Audier M, Pannetier J, Leblanc M, Janot C, Lang J M and Dubost B 1988 *Physica* B **153** 136
[28] Janot C, Pannetier J, Dubois J M and De Boissieu M 1989 *Phys. Rev. Lett.* **62** 450
Janot C, Dubois J M, Pannetier J, De Boissieu M and Fruchart R 1988 *Quasicrystalline Materials* ed C Janot and J M Dubois (Singapore: World Scientific) p 107
[29] Henley C L 1986 *Phys. Rev.* B **34** 797
[30] Audier M and Guyot P 1988 *Quasicrystalline Materials* ed C Janot and J M Dubois (Singapore: World Scientific) p 181
[31] Van Smaalen S 1989 *Phys. Rev.* B **39** 5850
[32] Elswijk H B, De Hosson J T M, Van Smaalen S and De Boer J L 1988 *Phys. Rev.* B **38** 1681
[33] Van Smaalen S 1989 *Proceedings of the NATO Advanced Workshop on 'Common Problems of Quasicrystals, Liquid Crystals and Incommensurate Insulator', Preveza* ed J C Toledano (New York: Plenum)
[34] Henley C L and Elser V 1986 *Phil. Mag. Lett.* B **53** L59
[35] Qiu S Y and Jaric M V 1989 *Proceedings of the Anniversary Adriatic Research Conference on Quasicrystals (Trieste, 1989)* ed M V Jaric and S Lundquist (Singapore: World Scientific) p 19
[36] Jaric M V 1986 *Phys. Rev.* B **34** 4685